Journal of Inorganic and General Chemistry
ZAAC
Zeitschrift für anorganische und allgemeine Chemie
www.zaac.wiley-vch.de
ARTICLE

DOI: 10.1002/zaac.201600325

Synthesis of Sb_2Se_3 and Bi_2Se_3 Nanoparticles in Ionic Liquids at Low Temperatures and Solid State Structure of $[C_4C_1Im]_3[BiCl_6]$

Manuel Loor,[a] Georg Bendt,[a] Julian Schaumann,[a] Ulrich Hagemann,[b] Markus Heidelmann,[b] Christoph Wölper,[a] and Stephan Schulz*[a]

Keywords: Bismuth; Antimony; Selenium; Thermoelectric material; Ionic liquids

Abstract. Crystalline Sb_2Se_3 nanoparticles were prepared by reaction of $SbCl_3$ with $(Et_3Si)_2Se$ in the presence of oleylamine (OA) in the ionic liquid $[C_4C_1Im]Cl$, whereas the reaction of $(Et_3Si)_2Se$ with $[C_4C_1Im]_3[BiCl_6]$ (**1**), which was obtained from the reaction of $BiCl_3$ with $[C_4C_1Im]Cl$ and structurally characterized by single-crystal X-ray diffraction, yielded Bi-rich Bi_2Se_3 nanoparticles. In contrast, the reaction of the reactive IL $[C_4C_1Im]_3[Bi_3I_{12}]$ with $(Et_3Si)_2Se$ in the presence of oleylamine in $[C_4C_1Im]I$ gave phase-pure Bi_2Se_3 nanoparticles. The chemical composition of the nanoparticles was investigated by EDX, while possible surface contaminations were studied by XPS and IR spectroscopy. The morphology of the nanoparticles was studied by SEM and TEM.

Introduction

Antimony and bismuth chalcogenides of the general type M_2E_3, (M = Sb, Bi; E = Se, Te) are promising materials for several technical applications including batteries,[1] photovoltaics and solar cells,[2] topological insulators (TIs),[3] and thermoelectric (TE) materials.[4] These applications often require nanostructured materials such as nanoparticles and thin films. Nanoparticles can be generally prepared either by top-down processes such as ball-milling or by bottom-up approaches, i.e. solvothermal routes, polyol processes, reduction reactions, and others, which have been established in the past for the size- and shape-selective synthesis of binary and ternary antimony and bismuth chalcogenides.[5]

Bismuth selenide Bi_2Se_3 is a small bandgap semiconductor with a direct bandgap, E_g = 0.35 eV,[6] whereas Sb_2Se_3 has an indirect energy bandgap of 1.21 eV and a direct transition at 1.22 eV according to very recent calculations.[7] The structure of Sb_2Se_3, which crystallizes in the space group *Pnma*,[8] can be described as one-dimensional chains along the direction of the *b* axis, which are cross-linked to give the 3D orthorhombic structure. Bi_2Se_3 crystallizes in the space group $R\bar{3}m$ (tetradymite type).[9] Both materials have received increasing interest in recent years as promising TE and TI materials. Sb_2Se_3 for instance shows a very high Seebeck coefficient (1800 $\mu V \cdot K^{-1}$), but its electrical conductivity ($\sigma \approx 10^{-6}$–10^{-2} $\Omega^{-1} \cdot m^{-1}$) unfortunately is very low.[10] However, electrical conductivity can be significantly enhanced by electrical doping for instance with Ag_2Se.[11]

Sb_2Se_3 nanoparticles with definite size and shape were typically synthesized by solvothermal processes,[12] microwave-assisted method,[13,14] and hot injection methods.[11] Recently, Sb_2Se_3 nanowires with diameters ranging from 10 to 20 nm and length up to 30 μm were prepared by reaction of triphenylantimony with dibenzyldiselenide.[15] Bi_2Se_3 nanoparticles were also obtained from polyol synthesis and microwave-assisted solvothermal routes, respectively.[16]

We are generally interested in the synthesis of nanostructured group 15 chalcogenide materials by gas-phase processes such as *metal organic chemical vapor deposition* (MOCVD)[17] and *atomic layer deposition* (ALD),[18] which were successfully applied in our group for the deposition of thin films of binary and ternary group 15 chalcogenides. Furthermore, we developed solution-based synthetic routes and synthesized crystalline Sb_2E_3 (E = S, Se, Te) and Bi_2Te_3 nanoparticles by thermal decomposition of metal organic (single source) precursors in high boiling organic solvents in the presence of capping agents such as PVP or oleylamine (OA).[19] In addition, ionic liquids (ILs) were successfully applied as novel solvent for the synthesis of Sb_2Te_3 nanoplates, which showed enhanced thermoelectric properties and high figure of merit values of up to 1.5.[20] The use of metal organic precursors allowed the material synthesis under kinetically controlled reaction conditions at low temperatures due to the weak metal-carbon bonds. Unfortunately, their low thermal stability, which is in particular true for Bi-containing compounds, often limits

* Prof. Dr. S. Schulz
Fax: +49-201-183-3830
E-Mail: stephan.schulz@uni-due.de
https://www.uni-due.de/ak_schulz/index_en.php
[a] Inorganic Chemistry and Center for Nanointegration Duisburg-Essen (CENIDE)
University of Duisburg-Essen
Universitätsstr. 5–7, S07 S03 C30
45117 Essen, Germany
[b] Interdisciplinary Center for Analytics on the Nanoscale (ICAN)
NETZ
Carl-Benz-Str. 199
47047 Duisburg, Germany
Supporting information for this article is available on the WWW under **http://dx.doi.org/10.1002/zaac.201600325** or from the author.

their applicability in material synthesis due to the occurrences of unwanted side reactions such as thermal decomposition reactions. For instance, the synthesis of Bi_2Te_3 was often accompanied by the formation of elemental Bi or Bi-rich phases as side-products. We became therefore interested in the development of alternative precursors and reaction processes.

We now report on the synthesis of phase-pure Sb_2Se_3 and Bi_2Se_3 nanoparticles by IL-based wet chemical approaches. The composition, phase purity and morphology of the materials were investigated by IR, EDX, XPS, XRD, SEM, and TEM and the solid-state structure of $[C_4C_1Im]_3[BiCl_6]$ (**1**) is discussed.

Results and Discussion

We recently reported on the synthesis and solid-state structure of $[C_4C_1Im]_3[Bi_3I_{12}]$, which was obtained in quantitative yield by reaction of equimolar amounts of $[C_4C_1Im]I$ and BiI_3, and its promising potential to serve as Bi source for the synthesis of phase-pure binary (Bi_2Te_3) and ternary ($[Bi_xSb_{1-x}]_2Te_3$) tetradymite-type metal telluride nanoparticles in an IL-based wet chemical approach.[21] In order to investigate the synthetic potential of this soluble and thermally stable Bi-source in more detail, we expanded our studies on the synthesis of the corresponding bismuth selenide Bi_2Se_3 (Scheme 1).

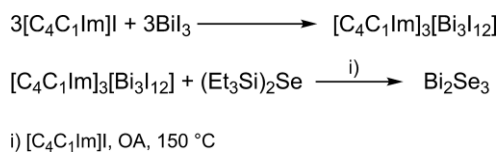

Scheme 1. Synthesis of Bi_2Se_3 nanoparticles.

$(Et_3Si)_2Se$ reacts with $[C_4C_1Im]_3[Bi_3I_{12}]$ in a solution of 10 mL of $[C_4C_1Im]I$ in the presence of OA at 150 °C with formation of a black precipitate, which was isolated by centrifugation and purified by repeatedly washing with acetonitrile and hexane (3 ×). The reaction also proceeded at lower temperatures such as 80 °C, but crystalline Bi_2Se_3 was only obtained at higher temperature. The soluble reaction products were further investigated by ^{29}Si NMR spectroscopy to identify the reaction mechanism (Figure 1).

$(Et_3Si)_2Te$ reacted with $[C_4C_1Im]_3[Bi_3I_{12}]$ in $[C_4C_1Im]I$ with formation of Et_3SiI (dehalosilylation reaction) and Si_2Et_6 (1:3 molar ratio), which was formed by homolytic cleavage of the Te–Si bond,[21] while the reaction proceeded with elimination of silylamine (Et_3SiOA) and Si_2Et_6 (2:1 molar ratio) in the presence of OA.[22] In contrast, the reaction of $(Et_3Si)_2Se$ with $[C_4C_1Im]_3[Bi_3I_{12}]$ in the absence of OA exclusively yielded Si_2Et_6, while Et_3SiOA and Si_2Et_6 (2:1 molar ratio) were formed in the presence of OA as was shown by ^{29}Si NMR spectroscopy (Figure 1A, B). The formation of Et_3SiI was not detected at all. These findings prove that OA is more reactive toward $(Et_3Si)_2Se$ compared to the iodide anion, while in the absence of OA, the homolytic Se–Si bond breakage reaction is preferred.

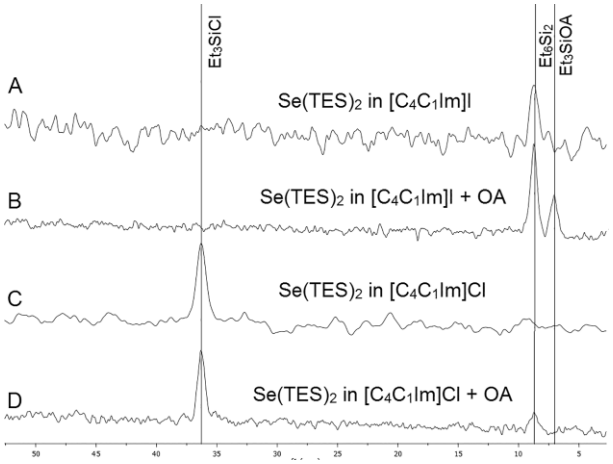

Figure 1. ^{29}Si NMR spectra of the products of the reaction of $(Et_3Si)_2Se$ with $[C_4C_1Im]_3[Bi_3I_{12}]$ (A, B) and $BiCl_3$ (C, D) at 150 °C.

The elemental composition of the resulting material as determined by EDX proved the formation of stoichiometric bismuth selenide Bi_2Se_3 (Table 1). According to IR spectroscopy studies, the material does not contain significant amounts of organic molecules as was shown by comparing the IR spectrum of the nanoparticles with those of pure OA, $[C_4C_1Im]I$, and acetonitrile (Figure 2).

Table 1. EDX results of Bi_2Se_3 and Sb_2Se_3.

	Bismuth /At%	Antimony /At%	Selenium /At%
Bi_2Se_3	40.5 ± 0.6	–	59.5 ± 1.5
Sb_2Se_3	–	42.5 ± 1.5	57.5 ± 1.0

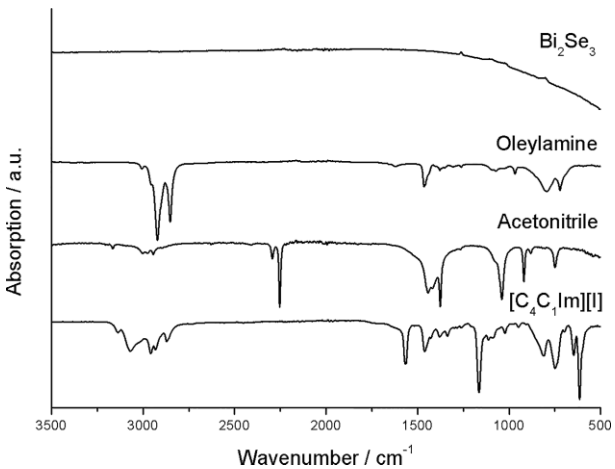

Figure 2. IR spectra of Bi_2Se_3 nanoparticles synthesized by reaction of $(Et_3Si)_2Se$ with $[C_4C_1Im]_3[Bi_3I_{12}]$ in $[C_4C_1Im]I$ in the presence of OA at 150 °C.

In contrast, XPS studies (Figure 3) prove the existence of carbon as well as a minimal amount of iodine, which most likely result from a residual IL layer on the surface of the nanoparticles. This thin surface layer cannot be detected by IR spectroscopy but by XPS due to the higher surface sensitivity. The binding energy of the main lines in the Bi and Se signals agree well with literature data of Bi_2Se_3 surfaces.[23] Selenium

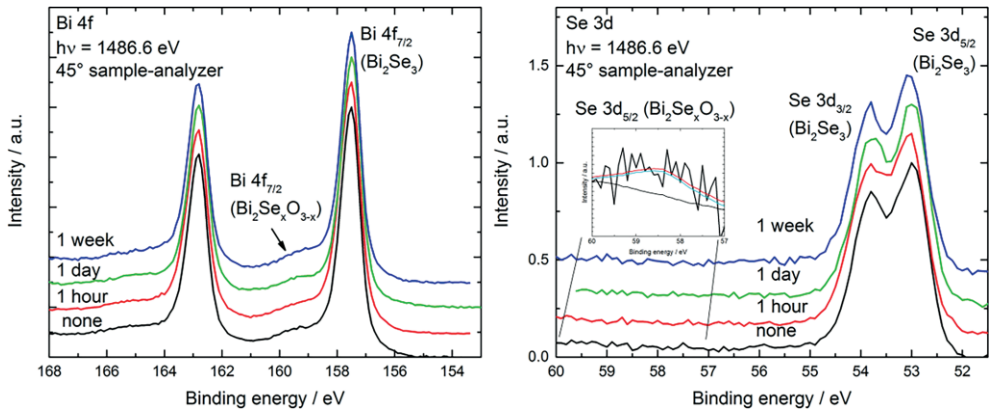

Figure 3. XPS Bi4f and Se 3d signals of Bi_2Se_3 nanoparticles synthesized by reaction of $(Et_3Si)_2Se$ with $[C_4C_1Im]_3[Bi_3I_{12}]$ in $[C_4C_1Im]I$ in the presence of OA at 150 °C. No change in the metal oxide content is visible upon exposure to air.

oxides (binding energy comparable to SeO_2) were hardly visible (see inlet Figure 3), while roughly 5 % of the Bi surface atoms are either present as bismuth oxides, most likely mixed bismuth oxoselenides $[Bi_2(O_xSe_{1-x})_3$, 90 %], or iodides (BiI_3 or BiOI, 10 %). The presence of bismuth oxides or iodides in these low quantities result in a shoulder to the large metal Bi signal and are not distinguishable.

The amount of bismuth and selenium oxides did not increase upon exposure to air. A very recent XPS study clearly revealed that Bi_2Te_3 and Bi_2Te_2Se easily form the corresponding oxides upon expose to air, while Bi_2Se_3 was significantly more stable.[24] Comparable findings were previously reported[25] and also observed for Bi_2Te_3 nanoparticles, which were shown to form bismuth oxides and tellurium oxides within a day upon expose to air.[21]

The material was also investigated by powder X-ray diffraction (PXRD), which clearly proved the formation of crystalline Bi_2Se_3 nanoparticles (Figure 4).

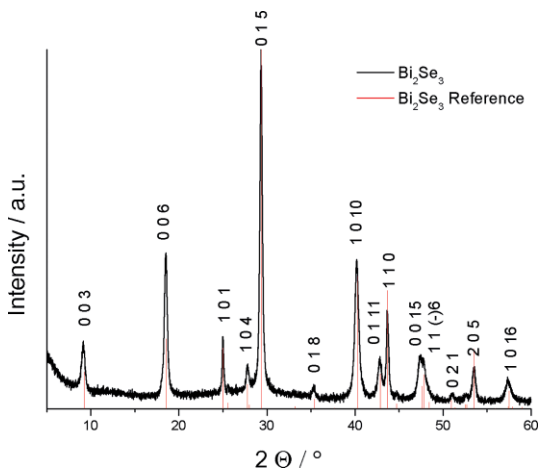

Figure 4. PXRD of Bi_2Se_3 nanoparticles synthesized by reaction of $(Et_3Si)_2Se$ with $[C_4C_1Im]_3[Bi_3I_{12}]$ in $[C_4C_1Im]I$ in the presence of OA at 150 °C and reference for Bi_2Se_3 (PDF 901-1965).[26]

The peaks can be indexed on the basis of phase-pure Bi_2Se_3 (PDF 901-1965). The lattice parameters were refined to a = 4.144(9) Å, c = 28.686(5) Å, and V = 426.8(3) Å^3, and are in good agreement with values reported for Bi_2Se_3 (PDF 901-1965). The XRD pattern shows a strong texture effect, since the hexagons arrange with the c axis perpendicular to the sample holder as was also observed in REM photographs (Figure 5). As a consequence, the intensity of the (00l) reflections is strongly enhanced as can be seen in particular for the (006) reflection, whereas the intensity of the (015) reflection is diminished compared to the standard card. In addition, the XRD pattern shows anisotropic peak broadening since the Bi_2Se_3 plates are relatively large (ca. 300 nm) but also very thin. For this reason, the XRD pattern shows strong peak broadening with exception of the (110) reflection at 43.8°.

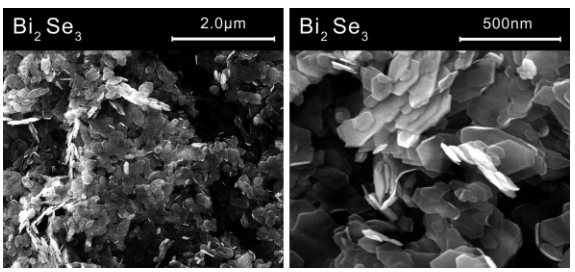

Figure 5. SEM image of Bi_2Se_3 nanoparticles synthesized by reaction of $(Et_3Si)_2Se$ with $[C_4C_1Im]_3[Bi_3I_{12}]$ in $[C_4C_1Im]I$ in the presence of OA at 150 °C.

The morphology of the Bi_2Se_3 nanoparticles was investigated by SEM and TEM. According to the SEM studies, the material contains largely agglomerated hexagonal Bi_2Se_3 nanoplates, whose size ranges from 50 to 500 nm (Figure 5). The agglomeration, which also indicates an almost capping-layer free surface, has been previously observed for Sb_2Te_3 and Bi_2Te_3 as well as $(Sb_xBi_{1-x})_2Te_3$ nanoparticles as-synthesized in ILs.[20,21] The shape and size of the hexagonal Bi_2Se_3 nanoplates is similar to those synthesized by other wet chemical bottom-up methods, which typically use shape and size controlling agents, and clearly results from the tetradymite-type layer structure. However, compared to standard capping agents such as oleylamine or PVP, the IL used herein obviously binds weaker to the surface and can therefore be easily washed away, resulting in the formation of largely agglomerated nanoparticles.[27]

TEM bright field images show the formation of hexagonal plates with sizes between 50 to 200 nm. A high-resolution high-angle annular dark-field (HAADF) image of the Bi_2Se_3 structure projected along the [5 10 1] direction is given in Figure 6 (right), clearly proving the crystalline nature of the material. The measured closest distance between two atomic columns is 0.29 nm, which is in good agreement to the value of 0.287 nm as reported in the literature.[28]

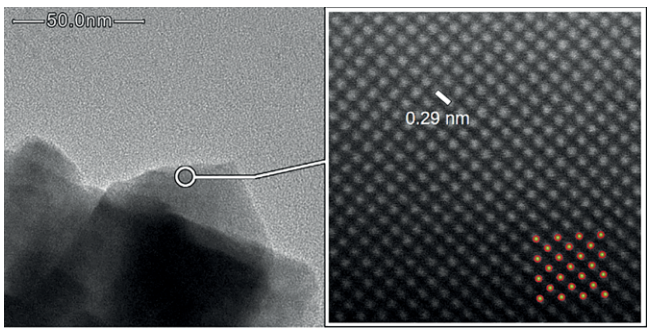

Figure 6. Conventional bright field TEM (left) and HAADF STEM (right) images of Bi_2Se_3 nanoparticles projected along [5 10 1] direction. Model structure of Bi_2Se_3 as overlay (orange: Bi, yellow: Se).

The use of the reactive IL $[C_4C_1Im]_3[BiI_{12}]$, which is easily obtained from the reaction of BiI_3 with an equimolar amount of $[C_4C_1Im]I$, in material synthesis avoids the formation of elemental bismuth or bismuth-rich material phases, i.e. BiTe or Bi_4Te_3 in case of bismuth tellurides, as is often observed in the synthesis of bismuth chalcogenides. This finding most likely results from its high reactivity but increased thermal stability compared to many (organometallic) bismuth sources. The reactions of $Se(SiEt_3)_2$ with $[C_4C_1Im]_3[BiI_{12}]$ were found to proceed at temperatures as low as 80 °C, which is higher than those with $Te(SiEt_3)_2$, which already occurred at ambient temperature, but below typical reaction temperatures as applied in polyol processes (up to 250 °C) and in reduction reactions or thermal decomposition reactions.[29] The higher reaction temperature in case of the reaction with $Se(SiEt_3)_2$ agrees with the decreasing *E*–Si bond energy (*E* = Se, Te) with increasing atomic number. However, in order to obtain highly crystalline material phases in a reasonable amount of time, reaction temperatures of 100 °C (Te) and 150 °C (Se) as well as prolonged reaction times of at least 2–3 h are necessary. Unfortunately, the homolytic *E*–Si bond breakage becomes more likely under these reaction conditions, which results in the formation of hexaethyldisilane Si_2Et_6. However, its formation can be fully avoided (*E* = Te) or suppressed (*E* = Se) if the reactions are performed in the presence of OA, which initially reacts with $E(SiEt_3)_2$ with formation of the silylamine (Et_3SiOA) and chalcogenide polyanions, which then smoothly react with $[C_4C_1Im]_3[Bi_3I_{12}]$ with formation of phase-pure Bi_2E_3.

To further expand the field of application of halogenidobismuthates as starting reagents in material synthesis, we investigated the reaction of $BiCl_3$ and $[C_4C_1Im]Cl$. The reaction with a threefold amount of $[C_4C_1Im]Cl$ yielded a liquid compound, from which a single crystal of $[C_4C_1Im]_3[BiCl_6]$ (**1**) was obtained by re-crystallization from a solution in ethanol. Compound **1** crystallizes in the orthorhombic space group $Pna2_1$ with two formula units in the asymmetric unit (Figure 7).

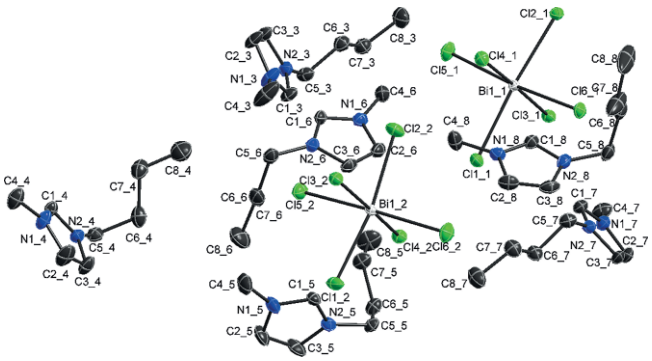

Figure 7. Solid state structure of $[C_4C_1Im]_3[BiCl_6]$ (**1**). Probability ellipsoids are displayed at 50 % probability levels and second disorder component hydrogen atoms are omitted for clarity. Selected bond lengths /Å and angles /°: Bi1_1–Cl6_1 2.6790(12), Bi1_1–Cl4_1 2.6906(11), Bi1_1–Cl2_1 2.7080(10), Bi1_1–Cl3_1 2.7191(10), Bi1_1–Cl1_1 2.7239(10), Bi1_1–Cl5_1 2.7404(11), Bi1_2–Cl4_2 2.6829(10), Bi1_2–Cl5_2 2.6845(13), Bi1_2–Cl1_2 2.6913(10), Bi1_2–Cl2_2 2.7155(10), Bi1_2–Cl3_2 2.7398(10), Bi1_2–Cl6_2 2.7643(12); Cl6_1–Bi1_1–Cl4_1 86.72(4), Cl6_1–Bi1_1–Cl2_1 85.87(4), Cl4_1–Bi1_1–Cl2_1 92.97(3), Cl6_1–Bi1_1–Cl3_1 89.97(4), Cl4_1–Bi1_1–Cl3_1 175.97(4), Cl2_1–Bi1_1–Cl3_1 89.08(3), Cl6_1–Bi1_1–Cl1_1 90.23(3), Cl4_1–Bi1_1–Cl1_1 89.37(3), Cl2_1–Bi1_1–Cl1_1 175.32(4), Cl3_1–Bi1_1–Cl1_1 88.35(3), Cl6_1–Bi1_1–Cl5_1 174.53(3), Cl4_1–Bi1_1–Cl5_1 90.40(4), Cl2_1–Bi1_1–Cl5_1 89.64(3), Cl3_1–Bi1_1–Cl5_1 93.09(4), Cl1_1–Bi1_1–Cl5_1 94.40(4), Cl4_2–Bi1_2–Cl5_2 87.24(4), Cl4_2–Bi1_2–Cl1_2 92.97(3), Cl5_2–Bi1_2–Cl1_2 85.75(4), Cl4_2–Bi1_2–Cl_22 94.62(3), Cl5_2–Bi1_2–Cl2_2 87.91(4), Cl1_2–Bi1_2–Cl2_2 169.87(4), Cl4_2–Bi1_2–Cl3_2 173.96(4), Cl5_2–Bi1_2–Cl3_2 86.97(4), Cl1_2–Bi1_2–Cl3_2 88.33(3), Cl2_2–Bi1_2–Cl3_2 83.44(3), Cl4_2–Bi1_2–Cl6_2 88.15(4), Cl5_2–Bi1_2–Cl6_2 175.34(4), Cl1_2–Bi1_2–Cl6_2 93.79(4), Cl2_2–Bi1_2–Cl6_2 93.16(4), Cl3_2–Bi1_2–Cl6_2 97.65(4).

The $BiCl_6^{3-}$ ions can be described as slightly distorted octahedra. Perpendicular to the *a* axis, the anions form layers of interconnected six-membered rings similar to those observed in the wurzite structure, however, the lower symmetry prevents a wurzite-type connection of the layers.

A closer inspection reveals that the opposing Bi–Cl bond lengths slightly differ (Bi1_1: mean 2.693 Å and 2.729 Å with differences ranging from 1.6 to 6.1 pm; Bi1_2: mean 2.686 Å and 2.740 Å with differences ranging from 2.4 to 8.0 pm) and that the differing Bi–Cl bond lengths are grouped in a *fac* arrangement. The *cisoid* Cl–Bi–Cl bond angles range from 85.87(4) to 94.40(4)° (Bi1_1) and 83.44(3) to 97.65(4)° (Bi1_2), and the transoid Cl–Bi–Cl bond angles deviate from linearity [Bi1_1: 174.53(3)–175.97(4)°; Bi1_2: 169.87(4)–175.34(4)°]. The deviation from linearity in the hexachlorobismuthate ion is comparable to that observed in other hexachlorobismuthates.[30] A statistical analysis of the CSD (mean difference of 10.5 pm with a std. deviation of 10 pm) shows absolute bond lengths ranging from 2.6790(12) to 2.7643(12) Å [CSD mean 2.71(6) Å], whereas the bond angles show the expected values for a slightly distorted octahedron (mean 90.00° and 174.17°).[31] However, considering the standard uncer-

tainties of the Bi–Cl bond lengths and the standard deviation of the CSD results, these findings, which match theoretical expectations, should not be overrated.

The hexachlorobismuthate(III) anion, a 14e system in which the electron lone pair formally shows a high (formally stereochemically inactive) s-character, often shows high variations (σ) in the Bi–Cl bond lengths and Cl–Bi–Cl angles. The distortion of the octahedral coordination of the $[BiCl_6]^{3-}$ anion has been traditionally explained as accommodating the spatial requirements of the electron lone pair, which points away from the shortest Bi–Cl bonds in the octahedron, while more recent studies addressed the distortion to the softness of this specific anion.[32] In addition, the variations can be significantly enhanced in case of the presence of intermolecular (weak) hydrogen bonding.[30c] *Orgel* attributed the structural distortion by mixing of the s and p orbital of the cation,[33a] which was confirmed by *Wheeler* and *Kumar* using extended Hückel calculations, according to which the trigonal distortion in the molecular anion $[BiCl_6]^{3-}$ results from the mixing of the cationic s orbital (HOMO) and the cationic p_z orbital (LUMO).[33b] This description implies that the lone pair electrons in $[BiCl_6]^{3-}$ on the central atom are hybridized toward the longer bonds and larger angles. In agreement with this description, the shorter Bi–Cl bonds Bi1_1-Cl2/4/6 and Bi1_2-Cl1/4/5 in **1** correspond to the smaller Cl–Bi–Cl angles, whereas the longer Bi–Cl bonds define the larger Cl–Bi–Cl angle. Alternatively, the bonding situation in the hexachlorobismuthate(III) anion can be formally described as asymmetrical 4e3c bond or as $BiCl_3$ with three additionally coordinated chloride anions.

Unfortunately, the reaction of $(Et_3Si)_2Se$ with $BiCl_3$ in a solution of $[C_4C_1Im]Cl$ in the presence of oleylamine did not yield phase-pure Bi_2Se_3. The reaction proceeded with elimination of Et_3SiCl (dehalosilylation) and formation of Si_2Et_6 (2:1 molar ratio) as shown in Figure 1D. Obviously, the chloride anion is far more reactive than the iodide anion, resulting in dehalosilylation (Figure 1C), while the less reactive iodide results in homolytic bond cleavage and formation of Si_2Et_6 (Figure 1A). Even though the XRD shows the formation of crystalline Bi_2Se_3 material in both cases, the resulting materials were Bi-rich according to EDX analysis (Bi 50 %, Se 50 %).

Since $[C_4C_1Im]_3[Bi_3I_{12}]$ was successfully applied for the synthesis of Bi_2Se_3 and Bi_2Te_3 nanoparticles,[21] we became interested to expand this procedure to the synthesis of the comparable antimony chalcogenides and turned our attention to the synthesis of antimony-containing reactive ILs. Halogenidoantimonates such as the $[Sb_3X_{11}]^{2-}$ dianions (X = Br, I) are well known and were found for instance in $[Cu(MeCN)_4]_2[Sb_3X_{11}]$.[34] We therefore investigated the reaction of SbI_3 with $[C_4C_1Im]I$, but we were not able to crystallize a specific halogenidoantimonate. The same was true for the reaction of $SbCl_3$ with $[C_4C_1Im]Cl$. We therefore turned our attention to the reaction of a mixture of SbI_3, $[C_4C_1Im]I$, and OA with $(Et_3Si)_2Se$, but this reaction only yielded a Sb-rich material phase according to EDX analysis (Sb 59 % Se 39 %, I 2 %) rather than the expected Sb_2Se_3. Even prolonged reaction times (24 h) and high reaction temperatures (200 °C) did not yield stoichiometric Sb_2Se_3. In remarkable contrast, the analogous reaction of $(Et_3Si)_2Se$ with $SbCl_3$ in $[C_4C_1Im]Cl$ and OA yielded phase-pure Sb_2Se_3, which was isolated as black precipitate and purified by repeatedly washing with acetonitrile and hexane (3 ×). ^{29}Si NMR spectroscopy studies again proved the formation of Et_3SiCl and Si_2Et_6 as was observed for the analogous reaction with $BiCl_3$ (Scheme 2).

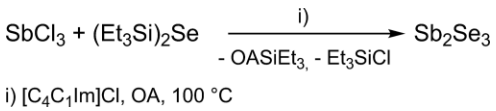

Scheme 2. Synthesis of Sb_2Se_3 nanoparticles.

The elemental composition of the material as determined by EDX proved the formation of highly stoichiometric Sb_2Se_3 (Table 1). PXRD studies clearly proved the formation of crystalline Sb_2Se_3 nanoparticles (Figure 8). The peaks can be indexed on the basis of phase-pure Sb_2Se_3 (PDF 901–7374). The determined lattice parameters [a = 1.163(2) nm, b = 0.397(6) nm, c = 1.168(1) nm] are in a very good agreement with the ICSD database for the pure orthorhombic Sb_2Se_3 phase. The XRD pattern shows strong preferred orientation of the needle-like Sb_2Se_3 structures. Compared to the standard card, the intensity of the (201), (302) and (402) reflections are strongly enhanced. The Sb_2Se_3 nanowires preferentially grow along the [010] direction as can be seen from the high intensity of the (h0l) reflections. This conclusion is supported by TEM and SAED and often observed for Sb_2Se_3 nanostructures.

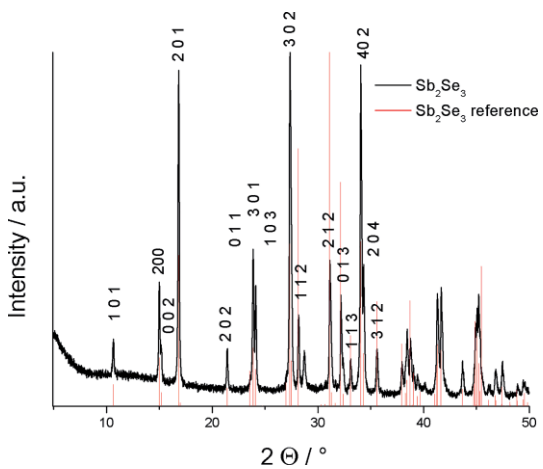

Figure 8. PXRD of Sb_2Se_3 nanoparticles synthesized by reaction of $(Et_3Si)_2Se$ with $SbCl_3$ in $[C_4C_1Im]Cl$ in the presence of OA at 150 °C and reference for Sb_2Se_3 (PDF 900-7374).[35]

IR spectroscopy (Figure 9) and XPS studies (Figure 10) revealed the existence of an organic capping layer. The carbon concentration is more pronounced than that observed for the Bi_2Se_3 particles. The binding energy of the main lines in the Sb and Se signals agree well with literature data of Sb_2Se_3 surfaces.[36] However, roughly 40 % of the Sb surface atoms of an *as-prepared* sample are present as antimony oxide or oxoselenide [Sb_2O_3 or $Sb_2(Se_xO_{3-x})_2$] but the oxygen content stays constant upon exposure to air. The oxygen signal at 532 eV binding energy increases strongly, showing the oxid-

ation of the capping layer and carbon contaminations on the surface. The Se 3d signal does show a small oxide peak only after one day of exposure to air. No further increase of the Se-oxide content is visible after that. However, the error in the determination of the Se-oxide [$Sb_2(Se_xO_{1-x})_3$] intensity is quite large, due to the weak signal and hence small signal to noise ratio.

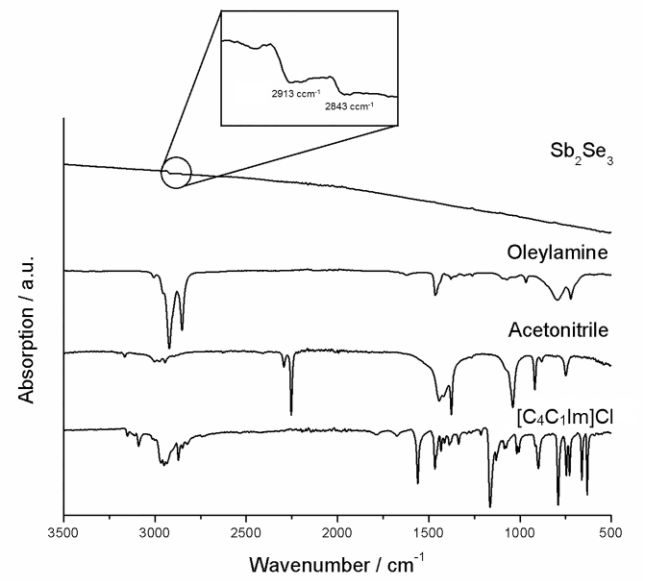

Figure 9. IR spectra of Sb_2Se_3 nanoparticles synthesized by reaction of $(Et_3Si)_2Se$ with $SbCl_3$ in $[C_4C_1Im]Cl$ in the presence of OA at 150 °C.

The morphology of the nanoparticles was investigated by SEM and TEM (Figure 11).

SEM photographs proved the formation of agglomerated Sb_2Se_3 nanowires with a high aspect ratio. They are up to 5 µm in length and show diameters of about 30 nm (Figure 11), which is comparable to those previously obtained by polyol processes (30–50 nm)[37] or by thermal decomposition of the *single source precursors* $(Et_2Sb)_2Se$ and Et_3SbSe.[19b]

Figure 12 shows HAADF STEM images of the Sb_2Se_3 nanowires. The nanowires have a big aspect ratio with lengths

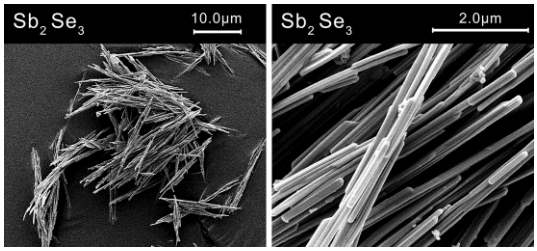

Figure 11. SEM image of Sb_2Se_3 nanoparticles synthesized by reaction of $(Et_3Si)_2Se$ with $SbCl_3$ in $[C_4C_1Im]Cl$ in the presence of OA at 150 °C.

up to 5 µm and diameters of about 30 nm. The Sb_2Se_3 nanowires are grown along the [010] direction of the stibnite structure in *Pnma* setting. A high-resolution image of a Sb_2Se_3 nanowire projected along the [001] direction is given in Figure 12 (right). Due to the contrast in HAADF mode being sensitive to the atomic number Z, atomic columns containing only Se can be distinguished from mixed SbSe columns. The measured distance of the (010) planes is 0.392 nm, which is in good agreement to value of d_{010} = 0.396 nm reported in the literature.[38] A model structure of Sb_2Se_3 is overlaid for comparison.

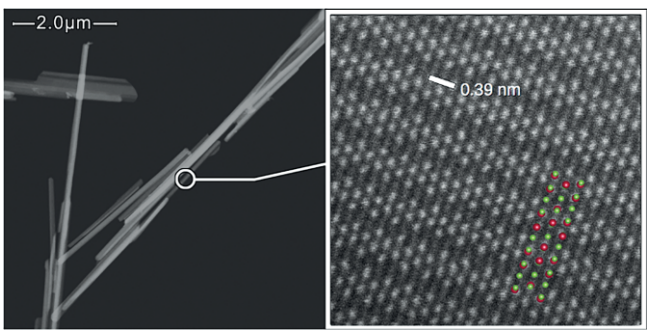

Figure 12. HAADF STEM images of Sb_2Se_3 nanoparticles in [001] orientation; structure model of Sb_2Se_3 as an overlay (red: Sb, green: Se).

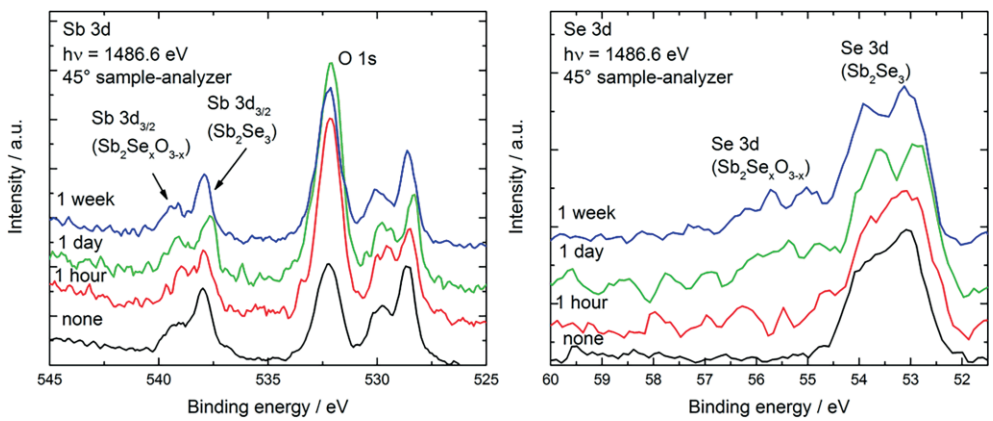

Figure 10. XPS Sb 3d and Se 3d signal of Sb_2Se_3 nanoparticles synthesized by reaction of $(Et_3Si)_2Se$ with $SbCl_3$ in $[C_4C_1Im]Cl$ in the presence of OA. The intensities of the signals do not change strongly upon exposure to air.

Conclusions

Phase-pure crystalline group 15 selenides M_2Se_3 (M = Sb, Bi) were synthesized under mild reaction conditions by reaction of $(Et_3Si)_2Se$ with $SbCl_3$ in $[C_4C_1Im]Cl$ or by reaction with the reactive IL $[C_4C_1Im]_3[Bi_3I_{12}]$ containing the trianionic halogenidobismuthate $[Bi_3I_{12}]^{3-}$. Both reactions were performed in the presence of oleylamine, which was found to effectively suppress the homolytic Se–Si bond cleavage reaction, and are scalable to produce of up to 10 g of the Sb_2Se_3 and Bi_2Se_3 nanoparticles. In contrast, the reaction of $(Et_3Si)_2Se$ with $[C_4C_1Im]_3[BiCl_6]$ (**1**), whose solid-state structure was determined by single-crystal X-ray diffraction, in the presence of oleylamine did not yield phase-pure Bi_2Se_3. The crystalline Sb_2Se_3 and Bi_2Se_3 nanoparticles are covered by a thin IL layer according to XPS results. The nanoparticles are relatively stable toward oxidation, in contrast to previously reported Bi_2Te_3 nanoparticles.[21] SEM and TEM studies proved the formation of largely agglomerated nanoparticles, which in case of Sb_2Se_3 nanowires exhibited a high aspect ratio. The use of the reactive Bi-containing IL $[C_4C_1Im]_3[Bi_3I_{12}]$ has the great advantage that the concentration of Bi, which must be provided for the formation of Bi_2Se_3, is relatively low. As a consequence, the formation of Bi-rich material phases or elemental bismuth is avoided.

Experimental Section

Synthetic procedures including the synthesis of the IL and thermolysis experiments were performed under inert gas conditions (argon atmosphere) in a glovebox or using standard Schlenk techniques. Acetonitrile (99.9+% extra dry, Acros), 1-chlorobutane (99%, ABCR), and *N*-methylimidazole (99+%, Sigma Aldrich) were commercially available and used as received, wheres ethyl acetate (J. T. Baker) was distilled prior to use. $(Et_3Si)_2Se$ was prepared according to a literature method.[39]

Synthesis of 1-Butyl-3-methylimidazolium Chloride $[C_4C_1Im]Cl$: In a 100 mL round-bottom flask 1-methylimidazole (8.1 mL, 10 mmol) and 1-butylchloride (13.5 mL, 13 mmol) were dissolved in acetonitrile (50 mL). The resulting solution was stirred at 60 °C for 5 d. Afterwards the solvent was removed in vacuo until a viscous, yellow oil was received. The oil was added dropwise to 200 mL ice-cooled and stirred ethyl acetate. The resulting white powder was separated by filtration, washed with further cool ethyl acetate and finally dried in vacuo. Yield: 16.77 g (96.5%). **^{1}H NMR** (300 MHz, 25 °C, $[D_6]$DMSO): δ = 9.20 (s, 1 H), 7.76 (dt, $^3J_{H,H}$ = 12.64, $^2J_{H,H}$ = 1.65 Hz, 2 H), 4.17 (t, $^3J_{H,H}$ = 7.2 Hz, 2 H), 3.86 (s, 3 H), 1.77 (dt, $^3J_{H,H}$ = 14.9, $^3J_{H,H}$ = 7.4 Hz, 2 H), 1.24 (dq, $^3J_{H,H}$ = 14.3, $^3J_{H,H}$ = 7.2 Hz, 2 H), 0.90 (t, $^3J_{H,H}$ = 7.3 Hz, 3 H) ppm.

Synthesis of 1-Butyl-3-methylimidazolium Iodide $[C_4C_1Im]I$: 1-Methylimidazole (22 mL, 0.276 mol) was dissolved in acetonitrile (100 mL), and 1-butyliodide (0.308 mol, 35 mL) was added dropwise in the dark at 0 °C. The solution was stirred at ambient temperature for 12 h and all volatiles were removed under dynamic vacuum. The resulting residue was washed with 150 mL of ethyl acetate. After removal of the solvent, the remaining yellowish oil was dried for 72 h under dynamic vacuum at 50 °C. Yield: 59.47 g (81%). **^{1}H NMR** (300 MHz, 25 °C, $[D_6]$DMSO): δ = 9.14 (s, 1 H), 7.76 (dt, $^1J_{H,H}$ = 13.5, $^2J_{H,H}$ = 1.7 Hz, 2 H), 4.19 (t, $3J_{H,H}$ = 7.2 Hz, 2 H), 3.88 (s, 3 H), 1.79 (dt, $^1J_{H,H}$ = 14.8, $^2J_{H,H}$ = 7.5 Hz, 2 H), 1.29 (m, 2 H), 0.93 (t, $^3J_{H,H}$ = 7.3 Hz, 3 H) ppm.

Synthesis of $[C_4C_1Im]_3[Bi_3I_{12}]$: $[C_4C_1Im]I$ (14.91 g, 0.561 mol) and BiI_3 (27.57 g, 0.468 mol) were added to ethanol (500 mL) and the resulting suspension was stirred at ambient temperature for 5 d. The resulting bright yellow solid was separated via filtration, washed with 100 mL of ethanol and carefully dried for 72 h under dynamic vacuum at ambient temperature. Yield: 30.87 g (77.16%). Melting point: 98 °C. Elemental analysis (EDX): Bi: 19.8 ± 1 at%, I: 80.2 ± 1.7 at%. **^{1}H NMR** (300 MHz, 25 °C, $[D_6]$DMSO): δ = 9.11 (s, 1 H), 7.73 (dt, $^1J_{H,H}$ = 20.2, $^2J_{H,H}$ = 1.8 Hz, 2 H), 4.16 (t, $^3J_{H,H}$ = 7.2 Hz, 2 H), 3.85 (s, 3 H), 1.76 (m, 2 H), 1.29 (m, 2 H), 0.93 (t, $^3J_{H,H}$ = 7.3 Hz, 3 H) ppm.

Synthesis of $[C_4C_1Im]_3[BiCl_6]$: $[C_4C_1Im]Cl$ (1.25 g, 7.18 mmol) and $BiCl_3$ (0.75 g, 2.37 mmol) were stirred at 120 °C for 4 h. The resulting highly viscous, white liquid was used without further purification. Yield: 2.0 g (100%). Elemental analysis (EDX): Bi: 13.8 ± 0.5 at%, Cl: 86.2 ± 2 at%. **^{1}H NMR** (300 MHz, 25 °C, $[D_6]$DMSO): δ = 9.41 (s, 1 H), 7.79 (dt, $^1J_{HH}$ = 20.3,, $^2J_{H,H}$ = 1.7 Hz, 2 H), 4.21 (t, $^3J_{H,H}$ = 7.2 Hz, 2 H), 3.89 (s, 3 H), 1.75 (m, 2 H), 1.23 (m, 2 H), 0.86 (t, $^3J_{H,H}$ = 7.3 Hz, 3 H) ppm.

Synthesis of $[C_4C_1Im]_3[SbCl_6]$: $[C_4C_1Im]Cl$ (1.40 g, 8.04 mmol) and $SbCl_3$ (0.60 g, 2.66 mmol) were stirred at 120 °C for 4 h. The resulting highly viscous, clear liquid was used without further purification. Yield: 2 g (100%). Elemental analysis (EDX): Sb: 14.9 ± 1.2 at%, Cl: 85.1 ± 1.6 at%. **^{1}H NMR** (300 MHz, 25 °C, $[D_6]$DMSO): δ = 9.38 (s, 1 H), 7.80 (m, 2 H), 4.18 (t, $^3J_{H,H}$ = 7.2 Hz, 2 H), 3.86 (s, 3 H), 1.75 (m, 2 H), 1.23 (m, 2 H), 0.87 (t,, $^3J_{H,H}$ = 7.3 Hz, 3 H).

Synthesis of Sb_2Se_3 Nanoparticles: In a centrifuge tube $SbCl_3$ (400 mg, 1.8 mmol), olelyamine (1 mL), and $[C_4C_1Im]Cl$ (4 g) were stirred at 100 °C for 30 min. $(Et_3Si)_2Se$ (200 µL, 0.7 mmol) was added to the resulting solution, and the mixture was thoroughly stirred. The black suspension was stirred at 150 °C for 12 h. The formed colloidal solution was centrifuged (2500 rpm) and washed with 6 × 15 mL acetonitrile. The separated particles were dried in vacuo at ambient temperature.

Synthesis of Bi_2Se_3 Nanoparticles: In a centrifuge tube $[C_4C_1Im]_3[Bi_3I_{12}]$ (1400 mg, 1.6 mmol), olelyamine (1 mL), and $[C_4C_1Im]I$ (4 g) were stirred at 100 °C for 30 min. $(Et_3Si)_2Se$ (200 µL, 0.7 mmol) was added to the resulting red solution, and thoroughly stirred. The black suspension was stirred at 150 °C for 12 h. The formed colloidal solution was centrifuged (2500 rpm) and washed with 6 × 15 mL acetonitrile. The separated particles were dried in vacuo at ambient temperature.

NMR Spectroscopy: ^{1}H (300 MHz) and $^{13}C\{^1H\}$ (75.5 MHz) NMR spectra (δ in ppm) were recorded with a Bruker Avance DPX-300 spectrometer and referenced to internal $[D_6]$DMSO (^{1}H: δ = 2.50; ^{13}C: δ = 39.51 ppm) or $CDCl_3$ (^{1}H: δ = 7.26; ^{13}C: δ = 77.16 ppm).

IR Spectroscopy: IR spectra were recorded in a glovebox with an ALPHA-T FT-IR spectrometer equipped with a single reflection ATR sampling module.

Single Crystal X-ray Diffraction: Crystallographic data of **1** were collected with a Bruker D8 Kappa APEX2 diffractometer (Mo-K_α radiation, λ = 0.71073 Å) at 100(2) K: $[C_{24}H_{45}BiCl_6N_6]$, M = 839.34, colorless crystal, (0.199 × 0.173 × 0.116 mm); orthorhombic, space group $Pna2_1$; a = 32.5929(14) Å, b = 12.6604(5) Å, c = 16.6457(7) Å; α =

90°, β = 90°, γ = 90°, V = 6868.7(5) Å^3; Z = 8; μ = 5.624 mm^{-1}; ρ_{calc} = 1.623 g•cm^{-3}; 196857 reflections (θ_{max} = 33.252°), 24997 unique (R_{int} = 0.0384); 695 parameters; Flack-Parameter x = 0.458(3); largest max./min in the final difference Fourier synthesis 1.300 e•Å^{-3}/ –0.986 e•Å^{-3}; max./min. transmission 0.48/0.27; R_1 = 0.0283 [$I > 2\sigma(I)$], wR_2 = 0.0526 (all data). The solid-state structure of **1** is shown in Figure 7. The structure was solved by Direct Methods (SHELXS-97)[40] and refined anisotropically by full-matrix least-squares on F^2 (SHELXL-2014).[41] Absorption corrections were performed numerical based on indexed faces (Bruker AXS APEX2). Hydrogen atoms were refined using a riding model or rigid methyl groups. The crystal was twinned by inversion and the model refined accordingly. One of the butyl groups is disordered over two positions. The minor compound could only be refined with a single mutual isotropic displacement parameter. The ADP of the major component suggests further disorder that could not be resolved.

Crystallographic data (excluding structure factors) for the structure in this paper have been deposited with the Cambridge Crystallographic Data Centre, CCDC, 12 Union Road, Cambridge CB21EZ, UK. Copies of the data can be obtained free of charge on quoting the depository number CCDC-1502363 for $[C_4C_1Im]_6[BiCl_6]_2$ (**1**) (Fax: +44-1223-336-033; E-Mail: deposit@ccdc.cam.ac.uk, http://www.ccdc.cam.ac.uk).

Powder X-ray Analysis: PXRD patterns were obtained with a Bruker D8 Advance powder diffractometer with Cu-K_α radiation (λ = 1.5418 Å, 40 kV and 40 mA) using a silicon single crystal as sample holder to minimize scattering. The powders were re-dispersed in ethanol on the silicon surface and investigated in the range from 10 to 90° 2θ with a step size of 0.01° 2θ with a counting time of 0.6 s. Rietveld refinement was performed with the program package TOPAS 5.0 (Bruker) to determine the lattice parameters and average crystallite size by use of the Scherrer equation with the program package TOPAS 5.0 (Bruker).[42] The background was modelled using Chebyshev polynomials. The structure models of Sb_2Se_3 (#85676) and Bi_2Se_3 (#72545) from the ICSD database were used. For each Rietveld refinement, the instrumental correction as determined with a standard powder sample from NIST (National Institute of Standards and Technology) as standard reference material [SRM 660b; a(LaB6) = 4.15689 Å] was taken into account.

XPS: XPS studies were performed with a Versaprobe II™ (Ulvac-Phi) with monochromatic Al-K_α light at 1486.6 eV photon energy. The emission angle between analyzer and sample is 45°. The Cu 2p signal at 932.67 eV binding energy of a sputter-cleaned Cu foil was used as the binding energy reference. The foil and the powder were put onto insulating double-sided tape and charging effects were compensated using a dual-beam neutralizing approach using electrons and slow moving argon ions.

Electron Microscopy: Particle size and morphology as well as elemental composition of the powders were analyzed by scanning electron microscopy (SEM) with a Jeol JSM 6510 microscope equipped with a Bruker Quantax 400 spectrometer (EDX, chemical composition). High-resolution STEM studies were carried out with a Jeol JEM 2200fs microscope equipped with probe-side Cs-corrector operated at 200 kV acceleration voltage.

Supporting Information (see footnote on the first page of this article): Spectroscopic data (NMR, IR) of $[C_4C_1Im]_3[BiCl_6]$ (**1**), $[C_4C_1Im]_3[SbCl_6]$, $BiCl_3$, $SbCl_3$, $[C_4C_1Im][Cl]$ and $[C_4C_1Im][I]$ as well as Rietveld refinements of Bi_2Se_3 and Sb_2Se_3 nanoparticles.

Acknowledgements

S. Schulz acknowledges financial support by the Deutsche Forschungsgemeinschaft (DFG) within the Priority Program *SPP 1708* "*Material Synthesis near Room Temperature*" and the University of Duisburg-Essen.

References

[1] a) D. Y. W. Yu, H. E. Hoster, *Sci. Rep.* **2014**, *51*, 4562/1–4562/6; b) D. Y. W. Yu, P. V. Prikhodchenko, *Nat. Commun.* **2013**, *4*, 2922–2928; c) P. V. Prikhodchenko, J. Gun, *Chem. Mater.* **2012**, *24*, 4750–4757.

[2] a) Y. C. Choi, T. N. Mandal, W. S. Yang, Y. H. Lee, S. H. Im, J. H. Noh, S. I. Seok, *Angew. Chem.* **2014**, *126*, 1353–1357; *Angew. Chem. Int. Ed.* **2014**, *53*, 1329–1333; b) F. T. F. O'Mahony, U. B. Cappel, N. Tokmoldin, T. Lutz, R. Lindblad, H. Rensmo, S. A. Haque, *Angew. Chem.* **2013**, ***125***, 12269 –12273; *Angew. Chem. Int. Ed.* **2013**, *52*, 12047–12051; c) J. A. Chang, J. H. Rhee, S. H. Im, Y. H. Lee, H.-J. Kim, S. I. Seok, M. K. Nazeeruddin, M. Grätzel, *Nano Lett.* **2010**, *10*, 2609–2612; d) B. Zhou, J. Zhu, *Nanotechnology* **2009**, *20*, 085604.

[3] a) W. Liu, Z. Zhang, X. Peng, J. Zhong, *Phys. B Cond. Matter* **2015**, *456*, 355–358; b) D. Koumoulis, B. Leung, T. C. Chasapis, R. Taylor, D. King Jr., M. G. Kanatzidis, L.-S. Bouchard, *Adv. Funct. Mater.* **2014**, *24*, 1519–1528; c) J.-J. Zhou, W. Feng, Y. Zhang, S. A. Yang, Y. Yao, *Sci. Rep.* **2014**, *514*, 3841/1–3841/6; d) Z. Xu, X. Guo, M. Yao, H. He, L. Miao, L. Jiao, H. Lin, J. Wang, D. Qian, J. Jia, W. Ho, M. Xie, *Adv. Mater.* **2013**, *25*, 1557–1562; e) Z. Wang, R. L. J. Qiu, C. H. Lee, Z. Zhang, X. P. A. Gao, *ACS Nano* **2013**, *7*, 2126–2131; f) J. Zhang, C.-Z. Chang, Z. Zhang, J. Wen, X. Feng, K. Li, M. Liu, K. He, L. Wang, X. Chen, Q.-K. Xue, X. Ma, Y. Wang, *Nat. Commun.* **2011**, *2*, 1588/1–1588/6; g) M. Z. Hasan, C. L. Kane, *Rev. Mod. Phys.* **2010**, *82*, 3045–3067; h) M. König, S. Wiedmann, C. Brüne, A. Roth, H. Buhmann, L. W. Molenkamp, X.-L. Qi, S.-C. Zhang, *Science* **2007**, *318*, 766–770; i) F. E. Camino, W. Zhou, V. J. Goldman, *Phys. Rev. Lett.* **2005**, *95*, 246802/1–4.

[4] a) H. S. Shin, B. Hamdou, H. Reith, H. Osterhage, J. Gooth, C. Damm, B. Rellinghaus, E. Pippel, K. Nielsch, *Nanoscale* **2016**, *8*, 13552–13557; b) G. L. Sun, L. L. Li, X. Y. Qin, D. Li, T. H. Zou, H. X. Xin, B. J. Ren, J. Zhang, Y. Y. Li, X. J. Li, *Appl. Phys. Lett.* **2015**, *106*, 053102; c) Z. Lu, L. P. Tan, X. Zhao, M. Layani, T. Sun, S. Fan, Q. Yan, S. Magdassi, H. H. Hng, *J. Mater. Chem. C* **2013**, *1*, 6271–6277; d) A. J. Minnich, M. S. Dresselhaus, Z. F. Ren, G. Chen, *Energy Environ. Sci.* **2009**, *2*, 466–479.

[5] a) Y. Zhang, G. D. Stucky, *Chem. Mater.* **2014**, *26*, 837–848; b) R. Benoit, V. Hornebecq, F. Weill, L. Lecren, X. Bourrat, M. Tregner-Delapierre, *Mater. Chem. A* **2013**, *1*, 14221–14226; c) M.-R. Gao, Y.-F. Xu, J. Jiang, S.-H. Yu, *Chem. Soc. Rev.* **2013**, *42*, 2986–3017; d) R. J. Mehta, C. Karthik, B. Singh, R. Teki, T. Borca-Tasciuc, G. Ramanath, *ACS Nano* **2010**, *4*, 5055–5060; e) G. Zhang, Q. Yu, X. Li, *Dalton Trans.* **2010**, *39*, 993–1004.

[6] B. Pejova, I. Grodzanov, A. Tanuševski, *Mater. Chem. Phys.* **2004**, *83*, 245–249.

[7] R. Vadapoo, S. Krishnan, H. Yilmaz, C. Marin, *Phys. Status Solidi B* **2011**, *248*, 700–705.

[8] a) N. W. Tideswell, F. H. Kruse, J. D. McCullough, *Acta Crystallogr.* **1957**, *10*, 99–102; b) G. P. Voutsas, A. G. Papazoglou, P. J. Rentzeperis, D. Siapkas, *Z. Kristallogr.* **2010**, *171*, 261–268; c) V. L. Deringer, R. P. Stoffel, M. Wuttig, R. Dronskowski, *Chem. Sci.* **2015**, *6*, 5255–5262.

[9] R. W. G. Wyckoff, *Crystal Structures*, 2nd ed., Krieger, Malabar, **1986**.

[10] a) X. W. Zheng, Y. Xie, L. Y. Zhu, X. C. Jiang, Y. B. Jia, W. H. Song, Y. P. Sun, *Inorg. Chem.* **2002**, *41*, 455–461; b) L. G. Gribnyak, T. B. Ivanova, *Inorg. Mater.* **1987**, *23*, 478–482; c) B. R.

Chakraborty, B. Ray, R. Bhattacharya, A. K. Dutta, *J. Phys. Chem. Solids* **1980**, *41*, 913–917.
[11] D. Choi, Y. Jang, J. Lee, G. H. Jeong, D. Whang, S. W. Hwang, K.-S. Cho, S.-W. Kim, *Sci. Rep.* **2014**, *51*, 6714/1–7.
[12] a) Y. Liang, Y. Wang, J. Wang, S. I. Wu, D. Jiang, J. Lian, *RSC Adv.* **2016**, *6*, 11501–11506; b) R. Jin, G. Chen, C. Yan, D. Chen, H. Xu, J. Pei, *CrystEngComm* **2012**, *14*, 8547–8553; c) L. Guo, G. B. Ji, X. F. Chang, M. B. Zheng, Y. Shi, Y. D. Zheng, *Nanotechnology* **2010**, *21*, 035606; d) Y. Chen, B. Deng, G. B. Cai, T. K. Zhang, W. F. Dong, W. X. Zhang, A. W. Xu, *J. Phys. Chem. C* **2008**, *112*, 672–679.
[13] Y.-Q. Liu, M. Zhang, F.-X. Wang, G.-B. Pan, *J. Mater. Chem. C* **2014**, *2*, 240–244.
[14] R. J. Mehta, C. Karthik, W. Jiang, B. Singh, Y. Shi, R. W. Siegel, T. Borca-Tasciuc, G. Ramanath, *Nano Lett.* **2010**, *10*, 4417–4422.
[15] G. Chen, W. Wang, C. Wang, T. Ding, Q. Yang, *Adv. Sci.* **2015**, *2*, 1500109.
[16] a) J. Buha, R. Gaspari, A. E. Del Rio Castillo, F. Bonaccorso, L. Manna, *Nano Lett.* **2016**, *16*, 4217–4223; b) M. Hong, Z.-G. Chen, L. Yang, G. Han, J. Zou, *Adv. Electron Mater.* **2015**, *1*, 1500025/1–9; c) A. Zhuang, J.-J. Li, Y.-C. Wang, X. Wen, Y. Lin, B. Xiang, X. Wang, J. Zeng, *Angew. Chem.* **2014**, *126*, 6543–6547; *Angew. Chem. Int. Ed.* **2014**, *53*, 6425–6429; d) Z. Lin, Y. Chen, A. Yin, Q. He, X. Huang, Y. Xu, Y. Liu, X. Zhong, Y. Huang, X. Duan, *Nano Lett.* **2014**, *14*, 6547–6553; e) H. Xu, G. Chen, R. Jin, D. Chen, Y. Wang, J. Pei, Y. Zhang, C. Yan, Z. Qiu, *CrystEngComm* **2014**, *16*, 3965–3970; f) Y. Min, G. D. Moon, B. S. Kim, B. Lim, J.-S. Kim, C. Y. Kang, U. Jeong, *J. Am. Chem. Soc.* **2012**, *134*, 2872–2875.
[17] a) G. Bendt, J. Sonntag, A. Lorke, W. Assenmacher, U. Hagemann, S. Schulz, *Semicond. Sci. Technol.* **2015**, *30*, 085021/1–7; b) G. Bendt, S. Schulz, S. Zastrow, K. Nielsch, *Chem. Vap. Deposition* **2013**, *19*, 235–241.
[18] a) C. Bae, T. Böhnert, J. Gooth, L. Seulky, S. Lee, H. Kim, S. Heimann, S. Schulz, H. Shin, K. Nielsch, *Semicond. Sci. Technol.* **2014**, *29*, 064003/1–7; b) S. Zastrow, J. Gooth, T. Böhnert, S. Heiderich, W. Töllner, S. Heimann, S. Schulz, K. Nielsch, *Semicond. Sci. Technol.* **2013**, *28*, 035010/1–6.
[19] a) M. Rusek, G. Bendt, C. Wölper, S. Schulz, *Eur. J. Inorg. Chem.* **2016**, 3673–3679; b) S. Heimann, W. Assenmacher, O. Prymak, S. Schulz, *Eur. J. Inorg. Chem.* **2015**, *14*, 2407–2415; c) G. Bendt, A. Weber, S. Heimann, W. Assenmacher, O. Prymak, S. Schulz, *Dalton Trans.* **2015**, *44*, 14272–14280; d) S. Schulz, S. Heimann, J. Friedrich, M. Engenhorst, G. Schierning, W. Assenmacher, *Chem. Mater.* **2012**, *24*, 2228–2234.
[20] S. Heimann, S. Schulz, J. Schaumann, A. Mudring, J. Stölzel, F. Maculewicz, G. Schierning, *J. Mater. Chem. C* **2015**, *3*, 10375–10380.
[21] M. Loor, G. Bendt, C. Wölper, W. Assenmacher, S. Schulz, *Dalton Trans.* **2016**, *45*, 15326–15335.
[22] S. Schulz, S. Heimann, K. Kaiser, O. Prymak, W. Assenmacher, J. T. Brüggemann, B. Mallik, A.-V. Mudring, *Inorg. Chem.* **2013**, *52*, 14326–14333.
[23] a) A. J. Green, S. Dey, Y. Q. An, B. O'Brien, S. J. O'Mullane, B. Thiel, A. C. Diebold, arXiv:1601.04057v1 [cond-mat.mtrl-sci]; b) C. D. Wagner, A. V. Naumkin, A. Kraut-Vass, J. W. Allison, C. J. Powell, J. R. Rumble Jr., NIST Standard Reference Database 20, Version 3.4. (web version) (http:/srdata.nist.gov/xps/).
[24] C. R. Thomas, M. K. Vallon, M. G. Frith, H. Sezen, S. K. Kushwaha, R. J. Cava, J. Schwartz, S. L. Bernasek, *Chem. Mater.* **2016**, *28*, 35–39.
[25] a) C. R. Thomas, G. Sahasrabudhe, S. K. Kushwaha, J. Xiong, R. J. Cava, J. Schwartz, *Phys. Status Solidi RRL* **2014**, *8*, 997–1002; b) L. V. Yashina, J. Sánchez-Barriga, M. R. Scholz, A. A. Volykhov, A. P. Sirotina, V. S. Neudachina, M. E. Tamm, A. Varykhalov, *ACS Nano* **2013**, *7*, 5181–5191; c) H. Bando, K. Koizumi, Y. Oikawa, K. Daikohara, V. A. Kulbachinskii, H. Ozaki, *J. Phys. Condens. Matter* **2000**, *12*, 5607–5616.
[26] S. Nakajima, *J. Phys. Chem. Solids* **1963**, *24*, 479–485.
[27] a) K. Kadel, L. Kumari, W. Li, J. Y. Huang, P. P. Provencio, *Nanoscale Res. Lett.* **2016**, *6*, 57; b) R. Harpness, A. Gedanken, *New J. Chem.* **2003**, *27*, 1191–1193.
[28] S. A. Semiletov, Z. G. Pinsker, *Dokl. Akad. Nauk SSSR* **1955**, *100*, 1079–1082.
[29] a) K. Kadel, L. Kumari, W. Li, J. Y. Huang, P. P. Provencio, *Nanoscale Res. Lett.* **2011**, *6*, 57/1–7; b) G. Zhang, W. Wang, X. Lu, X. Li, *Cryst. Growth Des.* **2009**, *9*, 143–150; c) R. Y. Wang, J. P. Feser, X. Gu, K. M. Yu, R. A. Segalman, A. Majumdar, D. J. Miliron, J. J. Urban, *Chem. Mater.* **2010**, *22*, 1943–1945; d) H. Cui, H. Liu, X. Li, J. Wang, F. Han, X. Zhang, R. I. Boughton, *J. Solid State Chem.* **2004**, *177*, 4001–4006.
[30] a) F. Wei, Z. Deng, S. Sun, F. Xie, G. Kieslich, D. M. Evans, M. A. Carpenter, P. D. Bristowe, A. K. Cheetham, *Mater. Horizon.* **2016**, *3*, 328–332; b) N. Elfaleh, H. Chouaib, S. Kamoun, *Acta Crystallogr., Sect. E* **2013**, *69*, m666; c) A. S. Rao, U. Baruah, S. K. Das, *Inorg. Chim. Acta* **2011**, *372*, 206–212; d) B. Zarychta, M. Bujak, J. Zaleski, *Z. Naturforsch. B* **2004**, *59*, 1029–1034.
[31] Cambridge Structural Database, Version 5.37, see also: F. H. Allen, *Acta Crystallogr., Sect. B* **2002**, *58*, 380–388. Analysis based on 44 hits including a $BiCl_6$ with co-ordination number of Cl set to 1. The opposing bond lengths were isolated by constraining the angle at Bi to be $<150°$.
[32] A. Guy Orpen, M. J. Quayle, *J. Chem. Soc., Dalton Trans.* **2001**, 1601–1610.
[33] a) L. E. Orgel, *J. Chem. Soc.* **1959**, 3815–3819; b) R. A. Wheeler, P. N. V. P. Kumar, *J. Am. Chem. Soc.* **1992**, *114*, 4776.
[34] a) S. Pohl, R. Lotz, W. Saak, D. Haase, *Angew. Chem.* **1989**, *101*, 355–357; *Angew. Chem. Int. Ed. Engl.* **1989**, *28*, 344–345; b) C. Vitzthumecker, A. Pfitzner, *Z. Anorg. Allg. Chem.* **2014**, *640*, 2366.
[35] R. Caracas, X. Gonze, *Phys. Chem. Minerals* **2005**, *32*, 295–300.
[36] a) G. Chen, J. Zhou, J. Zuo, Q. Yang, *Appl. Mater. Interfaces* **2016**, *8*, 2819–2825; b) C. D. Wagner, A. V. Naumkin, A. Kraut-Vass, J. W. Allison, C. J. Powell, J. R. Rumble Jr., NIST Standard Reference Database 20, Version 3.4. (web version) (http:/srdata.nist.gov/xps/).
[37] a) Z. Deng, M. Mansuripur, A. J. Muscat, *Nano Lett.* **2009**, *9*, 2015–2020; b) W. Tao, J. Wang, D. Wu, J. Chang, F. Wang, Z. Gao, F. Xu, K. Jiang, *Dalton Trans.* **2013**, *42*, 11411–11417; c) H. Zhang, M. Ge, L. Yang, Z. Zhou, W. Chen, Q. Li, L. Liu, *J. Phys. Chem. C* **2013**, *117*, 10285–10290.
[38] ICSD651518: O. M. Aliev, E. V. Magerramov, P. G. Rustamov, *Russ. J. Inorg. Chem. (Z. Neorgan. Khimii)* **1977**, *22*, 1539–1541.
[39] M. R. Detty, M. D. Seidler, *J. Org. Chem.* **1982**, *47*, 1354–1356.
[40] G. M. Sheldrick, *Acta Crystallogr., Sect. A* **1990**, *46*, 467–473.
[41] a) G. M. Sheldrick, *SHELXL-2014*, Program for the Refinement of Crystal Structures University of Göttingen, Göttingen, Germany **2014**; see also: G. M. Sheldrick, *Acta Crystallogr., Sect. A* **2008**, *64*, 112–122. shelXle, *A Qt GUI for SHELXL*: b) C. B. Hübschle, G. M. Sheldrick, B. Dittrich, *J. Appl. Crystallogr.* **2011**, *44*, 1281–1284.
[42] P. Scherrer, *Nachr. Ges. Wiss. Gött. Math.-Phys. Kl.* **1918**, *2*, 98–100.

Received: September 9, 2016
Published Online: ■